Structural Organization of Interphase 3T3 Fibroblasts Studied by Total Internal Reflection Fluorescence Microscopy

FREDERICK LANNI, ALAN S. WAGGONER, and D. LANSING TAYLOR
Center for Fluorescence Research in Biomedical Sciences and Department of Biological Sciences, Carnegie-Mellon University, Pittsburgh, Pennsylvania 15213

ABSTRACT We studied the laminar organization of 3T3 fibroblast cells growing on glass slides by use of total internal reflection illumination to excite fluorescence emission (TIRF) from labeled molecules and stained cellular compartments that are very close to the cell-substrate contact region. Mitochondria, distant from the contact regions and stained with the water-soluble cationic dye, dil-C_3-(3), fluoresced only as the glass/cytoplasm critical angle was approached. A similar result was obtained when the nuclei were stained with Hoechst dye 33342. From this measured angle a cytoplasmic refractive index in the range 1.358–1.374 was computed. The plasma membrane of 3T3 cells was stained with dil-C_{18}-(3), and the cytoplasmic compartment was stained with fluoresceinyl-dextran (FTC-dextran) or with carboxyfluorescein. We have demonstrated a high degree of correspondence between the low-reflectance zones in the reflection interference image of a live cell and the TIRF images of both the plasma membrane and cytoplasmic compartment. TIRF photometry of selected contact regions of cells provided data from which the absolute separation of cell and substrate was computed. From a population of 3T3 cells microinjected with fluorescein-labeled actin, motile and adherent interphase cells were selected for study. For adherent cells, which displayed fluorescent stress fibers, the TIRF image was composed of intense patches and less intense regions that corresponded, respectively, to the focal contact and close-contact zones of the reflection-interference image. The intense patches corresponded to the endpoints of the stress fibers. Cells of motile morphology, which formed some focal contacts and extensive close-contact zones, gave AF-actin TIRF images of relatively even intensity. Thin lamellar regions of the cytoplasm were found to contain concentrations of actin not significantly different from other close-contact regions of the cell. The major analytical problem of TIRF microscopy is separation of the effects of proximity to substrate, refractive index, and fluorescent probe concentration on the local brightness of the TIRF image. From our results, it appears possible to use TIRF microscopy to measure the proximity of different components of substrate contact regions of cells.

Mammalian fibroblasts that are grown on a planar substrate exhibit a laminar morphology that is a result of spatial constraints and the forces of adhesion and motility. Cell-substrate contacts are classified by degree of apposition and by size. Reflection-interference microscopy (1–3) and electron microscopy (4) have been used to demonstrate the existence of close contacts (extended domains in which the distance between cell membrane and substrate is ~50 nm) and focal contacts (compact domains in which the separation may be as little as 10 nm).

The distribution and interaction of the cytoskeletal and contractile proteins responsible for cell-substrate attachments and, by implication, the sites of application of forces to the substrate are now partly understood (for a review, see Geiger [5]). Electron microscopy, immunofluorescence microscopy, and fluorescent analogue cytochemistry demonstrate that ac-

THE JOURNAL OF CELL BIOLOGY · VOLUME 100 APRIL 1985 1091-1102

tin-containing stress fibers terminate at focal contacts (4–10). There is also data indicating that vinculin in focal contacts is closer to the cytoplasmic surface of the plasma membrane than either α-actinin or tropomyosin (7, 11, 12).

Cellular functions such as cell movement, endocytosis, exocytosis, and division probably involve changes in the distribution and interaction of specific molecules and organelles. These changes occur not only in the plane of the substrate but also in the dimension normal to the substrate. Therefore, it is important to analyze the activity and distribution relative to the substrate of specific molecules and organelles in living cells during normal function.

Fluorescence techniques have become important tools in the study of molecular dynamics in cells. Fluorescent probes have been developed that are specific for certain macromolecules (13), organelles (14, 15), compartments (16), and physiologically important parameters, such as membrane potential (17–19), pH (20), pCa (21), and specific enzymes (22). The development of fluorescent analogue cytochemistry has made possible the study of specific molecules and specific molecular interactions in living cells (23–25). Finally, various quantitative fluorescence microscopic techniques have greatly increased the number of molecular and systemic parameters accessible to measurement in and on cells (25–32).

Total internal reflection fluorescence (TIRF)[1] microscopy has been demonstrated by Axelrod (33) to be a technique applicable to the study of cell-substrate contact. In the phenomenon of total internal reflection (TIR), an electromagnetic wave that is incident on a high-to-low refractive index interface at an angle that exceeds the critical angle is 100% reflected at the interface. This produces an electromagnetic disturbance, the evanescent field, in the low-index medium that typically extends only a fraction of a wavelength beyond the interface. A suitable dye molecule in the low-index medium will absorb energy from this evanescent field and luminesce if it is located close to the interface. In general, a resonant molecule in the low-index medium will absorb and scatter radiation from the evanescent field. A refractive inhomogeneity also will scatter radiation from the field. In microscopic applications, the high-index medium is typically glass and the low-index medium is the specimen; cells growing in culture medium on the surface of a microscope slide. With this kind of specimen, the angle of incidence of the illumination can be conveniently adjusted so that the evanescent-field strength is significant only within 100 nm of the interface. This limits penetration of the field only into the cell-substrate contact regions.

The present study combines the use of specific probes of organelles and compartments, the fluorescent analogue of actin, and TIRF microscopy to analyze the organization of interphase 3T3 cells grown on glass substrates.

MATERIALS AND METHODS

Chemicals: 5-Iodoacetamido fluorescein and carboxyfluorescein diacetate (CFD) were obtained from Molecular Probes, Inc. (Junction City, OR). CFD was a mixture of 5- and 6-carboxy isomers and was used to prepare a 3 mg/ml stock solution in ethanol. 6-Carboxyfluorescein was obtained from Eastman Kodak Co. (Rochester, NY). Hoechst Dye 33342 was obtained from Calbiochem-Behring (San Diego, CA), and fluorescein-labeled dextran (FTC-dextran) (FD-70S; average molecular weight = 6.6×10^4) was obtained from Sigma Chemical Co. (St. Louis, MO). The indocarbocyanine dyes 3,3′-dipropylindo tricarbocyanine (dil-C_3-[3]) and 3,3′-dioctadecylindo tricarbocyanine (dil-C_{18}-[3]) were prepared using iodopropane and iodooctadecane, respectively, in the procedure outlined by Sims et al. (17).

Cell Culture: Swiss 3T3 cells from American Type Culture Collection (Rockville, MD) were grown at 37°C in 5% CO_2 in flasks containing Dulbecco's modified Eagle's medium (DME) supplemented with calf serum (10%), penicillin, streptomycin, and L-glutamine (Gibco Laboratories, Grand Island, NY). Serial culture passage number for these cells ranged from 125 to 134. 1 or 2 d before use, cells were removed from the flask by treatment with trypsin and EDTA in buffered saline, and replated on Gold Seal slides (Clay Adams, Parsippany, NJ) at a density of 5×10^3 cm^{-2} and were used the next day when the number had roughly doubled. For microscopy, HEPES-buffered Dulbecco's modified Eagle's medium without serum or other supplements was used. The refractive index for this culture medium was measured at room temperature (23°C) to be 1.335. The microscope slide refractive index was 1.5162, computed from photometric measurements of slide transmission at 488 nm.

Preparation and Introduction of Labeled Actin: Fluorescein-labeled actin (AF-actin) was prepared from 5-iodoacetamidofluorescein and rabbit skeletal muscle actin by the procedure of Wang and Taylor (34). Concentrated solutions of depolymerized AF-actin (5 mg/ml in "injection buffer": 2 mM PIPES, 0.1 mM ATP, 0.1 mM dithiothreitol, 50 μM $MgCl_2$, pH 7.0 at 23°C) were clarified by centrifugation. Actin was microinjected into 3T3 cells growing on slides as described previously (35). The volume of actin solution introduced by this procedure has been estimated to be 5–10% of the cytoplasmic volume. After introduction of AF-actin into the cells, each slide was submerged in complete Dulbecco's modified Eagle's medium and incubated at 37°C in 5% CO_2 for several hours before examination.

Introduction of Dextran: The FTC-dextran was used after dialysis or without further purification. Cells were microinjected as described above for AF-actin, or were loaded in large numbers on the day before an experiment by the method of McNeil et al. (36). Cells loaded with dextran showed diffuse fluorescence of the cytoplasmic compartment, and exclusion from major vesicular organelles. Dextrans of >40,000 mol wt were excluded from the nucleus during the several hours necessary for each experiment.

Mitochondrial Stain: dil-C_3-(3) is a water-soluble indocarbocyanine dye that will permeate membrane-enclosed compartments. Because it is a cation, it accumulates in electronegative compartments, and, therefore, stains the cytoplasm weakly and the mitochondria intensely relative to the external medium. The absorption (553-nm peak) and emission bands of this dye, like other dil-(3), are well-matched to the "rhodamine" fluorescence optics. For TIRF, an excitation wavelength of 514 nm was used, and emission was measured in the band >590 nm.

Staining Procedures: Mitochondria were stained by adding dil-C_3-(3) to a final concentration of 5×10^{-8} M in 1–2 ml culture media. Cells were exposed to this dye solution for 20 min, after which the cells were rinsed with fresh culture media. The membrane stain dil-C_{18}-(3) was dispersed into culture media from a small amount of ethanol. Background staining was more severe with this dye when older cultures were used, apparently because of cellular material deposited on the glass surface during normal migration of 3T3 cells. Cells were incubated with the stain for 5 min, then rinsed with fresh media. The DNA-specific probe Hoescht dye 33342 was dissolved in water and a small amount of this solution was added to culture media for staining (final concentration = 20 μg/ml). Cells were rinsed after a 5-min incubation with the dye. As a cytoplasmic marker, carboxy-fluorescein was introduced into cells by adding the diacetate (CFD) in 1.0 μl of ethanol to 2–3 ml of fresh culture media without serum (final dye concentration = 6 μM). Cells were exposed to CFD for 1–10 min, after which they were rinsed with fresh media.

The contact regions of cells could also be examined by bright-field TIRF produced simply by adding membrane-impermeant dye to the media external to the cells. TIRF was then excited evenly over the entire glass/media interface, except for locations where cell contact limited the thickness of the film of culture medium between cell and glass to less than the attenuation distance of the evanescent field. Clear reversed-contrast TIRF images were obtained. The external dye could then be readily removed by rinsing the cells, and a second stain applied (data not shown).

Theory and TIRF Instrumentation: In our experiments, TIR of a collimated monochromatic beam of light occurred at the interface between a glass microscope slide optically coupled to a prism (n_1 = 1.5222) and cell culture medium (n_2 = 1.335). The critical angle for this pair of substances is 61.3°. For incidence angles greater than the critical angle, essentially no refracted light is propagated in the second medium. Instead, a nonpropagating electromagnetic field is induced in the second medium that has the same frequency

[1] *Abbreviations used in this paper:* AF-actin, fluorescein-labeled actin; CFD, carboxyfluorescein diacetate; dil-C_3-(3), 3,3′-dipropylindo tricarbocyanine; dil-C_{18}-(3), 3,3′-dioctadecylindo tricarbocyanine; FTC-dextran, fluorescein-thiocarbamoyl-dextran; TIR, total internal reflection; and TIRF, total internal reflection fluorescence.

as the incident light (37, 38). The intensity of this evanescent field is attenuated exponentially with distance measured from the substrate (z):

$$I(z) = I(0)\exp(-z/d). \quad (1)$$

The attenuation constant (d) is a function of wavelength (λ *in vacuo*), angle of incidence (θ), and refractive index:

$$d_{12}(\theta) = (\lambda/4\pi)(n_1^2\sin^2\theta - n_2^2)^{-1/2}. \quad (2)$$

For s-polarized incident light the evanescent field will also be s-polarized with the surface intensity ($I[0]$) proportional to $\cos^2\theta/(n_1^2 - n_2^2)$. It should be noted that the numerical value of the attenuation constant is unaffected by refractive index mismatch between the prism and microscope slide since the incidence angle appears in the expression for $d(\theta)$ as $n_1 \cdot \sin\theta_1$, which is equal to the product n(slide) · sin θ(slide) by Snell's Law. In contrast, $I(0)$ will be a function of slide refractive index, and the true incidence angle in the slide must be used in the expression for $I(0)$. The excitation intensity at the specimen/slide interface must also be corrected for angle-dependent reflective losses at the air/prism, prism/oil, and oil/slide interfaces.

Under typical conditions, the attentuation constant will be a fraction of a wavelength: for λ = 488 nm and θ = 75.7°, d = 62 nm. A fluorescent dye molecule in the second medium will be excited and luminesce at a rate proportional to the local field intensity, $I(z)$. Therefore, in a fluorescent specimen, only those dye molecules located within a few attenuation lengths of the interface will contribute to TIRF emission or the TIRF image (33, 39). The apparent simplicity of Eq. 1 is complicated by the fact that the induced electromagnetic fields of the dye molecules, and of other refractive particles in the specimen, perturb $I(z)$ due to partial reflection of the fields at the interface, and due to proximity of the dye molecule to other scattering particles. Furthermore, the directional probability of fluorescence emission from a molecule near a dielectric interface is in general not isotropic, even when the average orientation of the emission dipole is isotropic (40–42). This is due to interference between emitted waves and waves reflected from the interface, and also due to evanescent waves in the molecule's near field which appear as homogeneous plane waves close to the critical angle in the more-refractive substrate. However, for the relative refractive indices encountered in these specimens, the greatest of which is 1.1357 (the ratio of n[slide] to n[medium]), the reflective perturbation of $I(z)$ is small. Likewise, for emission into the entrance aperture of a microscope located on the specimen (lower refractive index) side of the interface, the interference effect is small. The perturbation of $I(z)$ at the location of a dye molecule by other scatters (such as protein molecules) varies as the sixth power of their separation. This would be a major effect if the average separation of particles was ≤1 nm. In cytoplasm, where the concentration of macromolecules is ~200 mg/ml, the average separation of particle centers is roughly 8 nm. In this case, the field intensity acting on a dye molecule due to other scatterers is about four orders of magnitude less than the intensity of the driving field, $I(z)$. The partitioning of emitted power between homogeneous plane waves and evanescent waves coupled to plane waves in the substrate is a strong function $W(z)$ of the distance between the emitting molecule and the interface. Approximate analytical expressions derived by Lukosz and Kunz (43) can be used to correct TIRF photometric data for this effect. In this report we have made this correction, and have otherwise assumed that the detected fluorescence emission is proportional to $I(z)$, for the reasons outlined above.

The instrument used in these experiments (Fig. 1) was designed around a Zeiss Universal microscope equipped for epifluorescence. In place of the stage was a glass cube prism mounted on micrometer slides (Klinger Scientific, Jamaica, NY) allowing lateral translation of the specimen as well as vertical focusing. The prism was made by cementing together two right-angle prisms of BK-7 glass (Melles Griot, Irvine, CA) to form a 1-inch cube of refractive index 1.5222. The specimen slide was coupled to the top of the prism with immersion oil (n = 1.515), and the microscope objective lens (40X or 63X) was coupled to the specimen by immersion in the culture medium. Images were recorded on videotape from a SIT video camera (RCA TC1030/H) for fluorescence or a Newvicon camera (Dage NC65SX) for reflection interference). The principal light source for TIRF was an argon ion laser (Model 165, Spectra-Physics Inc., Mountain View, CA) the collimated beam of which was directed into the prism by a moveable mirror that allows for adjustment of the angle of incidence. The beam entering the prism was s-polarized, thus producing a field of the same polarization in the specimen. For excitation of Hoechst dye 33342, unpolarized, collimated ultraviolet light (365 nm) from a mercury arc lamp followed the same route to the specimen. It was relatively convenient to switch between fluorescence, TIRF, and reflection-interference modes.

TIRF Intensity and Absolute Separation of Specimen and Substrate: The fluorescence intensity at any particular location in the TIRF image of a cellular specimen will generally be a function of three local specimen parameters; proximity to substrate, refractive index, and fluorescent dye concentration. In the simplest case of a cell that has the same refractive index as the external medium and is homogeneously labeled on the membrane or in the cytoplasmic volume, the TIRF image will be a map of only the proximity of cell and substrate. A single TIRF image does not, however, map absolute distance. Because the intensity of the evanescent field in the specimen is an exponential function of distance, a cell that contacts the substrate and an identical cell displaced away from the substrate give TIRF images that differ only in brightness, not in pattern. The TIRF intensity measured at a particular location in a TIRF image will be proportional to the integrated product of dye concentration $c(z)$, evanescent-field intensity $I(z)$, and the weighting function $W(z)$, over the range z_p to z_d, where z_p is the boundary of the labeled specimen compartment proximal to the substrate, and z_d is the distal boundary (here assumed to be $\gg d[\theta]$). The absolute distance, z_p, between the substrate and the labeled cell compartment can be computed from the ratio of the TIRF intensities at one location measured at a minimum of two incidence angles θ_1 and θ_2. The relation between z_p and measured fluorescence intensity is given in the appendix to this report.

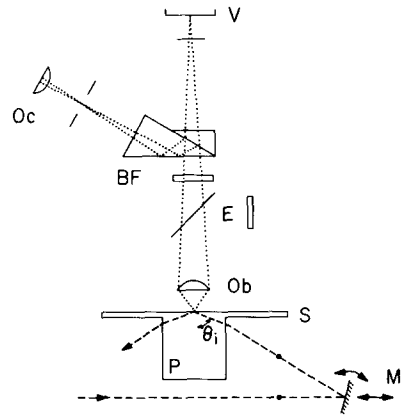

FIGURE 1 Schematic diagram of TIRF microscope. A standard fluorescence microscope is equipped with a glass cube prism (*P*) on micrometer translators. The specimen slide (*S*) is optically coupled to *P* with immersion oil. A collimated s-polarized beam from an argon-ion laser or other light source is totally reflected from the slide-specimen interface at an angle θ_i adjusted by mirror *M*. The specimen is coupled to the microscope objective lens (*Ob*) by immersion in the cell culture medium of the specimen. The episcopic illuminator (*E*) is used for fluorescence excitation or reflection interference. Operation can be quickly switched between TIRF, reflection-interference, and fluorescence modes. A barrier filter (*BF*) is used in the TIRF mode to absorb radiation scattered from the evanescent field. A video camera (*V*) is located with the photocathode in the primary image plane of the microscope. For photometry, the image-plane diaphragm of a photomultiplier photometer is used in place of *V*. Direct viewing is through oculars (*Oc*).

The simplest optical model is one in which the specimen has a single refractive index. We have extended the theory of TIR to a more realistic model having four layers ([1] glass: [2] culture medium: [3] membrane: [4] cytoplasm) of refractive index $n_1 > n_3 > n_4 > n_2$. The parameter of interest here is z_2, the distance between the substrate and the bilayer membrane of the cell. In our data analyses, the bilayer membrane was treated as a dielectric layer of index 1.400, equal to that of dodecane, and a thickness (z_3) of 4.0 nm. A significant fraction of protein in the membrane at contact zones could increase the index (n_3) significantly.

3T3 cells growing on glass slides were stained with carboxyfluorescein diacetate or loaded with FTC-dextran. Cells were examined by reflection-interference microscopy and regions of medium- or low-reflectance were located. Low-reflectance regions were generally compact as expected for focal attachments and fit entirely within the photometer field. Medium-reflectance regions were generally large as expected for close contacts and the photometer field could be placed entirely within the boundary. Microphotometric measurements of fluorescence emission were made at these locations using wide-field illumination at a wavelength of 488 nm, and an emission passband of 520–560 nm. The first measurement was made with the illumination incidence angle set to 75.20° in the prism, the second measurement at 69.43°. Background emission was then estimated at the same incidence angles after moving the cell out of the detector field. To limit exposure of the specimen, we used only two incidence angles, even though more information can be derived from a more complete graph of emission vs. incidence angle. Measured fluorescence emission

was corrected by subtraction of background, and normalized for angle-dependent reflective loss of excitation power at the prism entrance face and the prism/slide interface. The normalized-emission ratio, $F(2)/F(1)$, was averaged separately for focal contacts and close-contact zones, and this average ratio used in the computation of z_2, the separation of substrate and plasma membrane, at these sites.

Time-lapse Measurements: Cells injected with AF-actin were maintained at ~36°C by directing a stream of warm air at the prism and lower surface of the specimen slide on the microscope. Culture medium was replaced periodically to compensate for evaporation. At 15-min intervals, the TIRF, reflection-interference, and fluorescence images were recorded in rapid succession so as to limit the radiation dose received by the cells of interest.

Reflection-Interference Microscopy: The reflection-interference image (1, 3) was generated at 546 nm by using the epifluorescence illuminator with the "rhodamine" exciter filter and "FITC" reflector/barrier filters in the optical path. The video camera threshold and gain properties are such that considerable contrast enhancement occurs relative to the image observed directly. "Close" and "focal" contact regions were identified as medium-reflectance and compact low-reflectance image regions respectively. Quantitative analysis of these images was not attempted. The reflection-interference images were recorded at nearly full illumination aperture so that the contrast of the first order fringes due to reflections from the substrate and upper surface of the cell was minimized relative to the contrast of the zero-order pattern of cell-substrate contact (44, 45).

Comparison of Surface TIRF, Volume TIRF, and Reflection-Interference Images: A result of the exponential relationship between TIRF and substrate proximity is that the TIRF image of a homogeneously surface-stained object will be everywhere proportional to the volume-stain TIRF image of that same object. Refractive index mismatch between culture medium, membrane, and cytoplasm, or extreme thinness of the specimen, will complicate strict identity between the two images. To test the above relationship and to determine that the plasma membrane and cytoplasmic compartment at least follow the same contour, we first membrane-stained 3T3 cells with dil-C_{18}-(3) and the "red" TIRF image was then recorded. This was followed by in situ staining of the cytoplasmic compartment with CFD and recording of the "green" TIRF image. The zero-order reflection interference image of the cell was also recorded. Locations of intense TIRF should also be locations of low reflectivity under these conditions.

RESULTS

TIR Refractometry and Proximity of Mitochondria and Nuclei to Substrate

TIRF images (d = 60–100 nm) of entire fields of cells stained with dil-C_3-(3) showed only an occasional mitochondrion located close enough to the substrate to be significantly fluorescent. To increase the penetration of the evanescent field into the cytoplasm, we decreased the angle of incidence until it was close to the critical angle. Appearance of fluorescent mitochondria occurred sharply at an incidence angle of 63.0°–64.4°. Scattering of light by the adherent cells also increased sharply in the same range suggesting that the critical angle for the glass/cytoplasm boundary had been attained. At higher incidence angles, only background staining and weak, diffuse fluorescence from dil-C_3-(3) in the cytoplasm was detected (Fig. 2). From the known refractive index of the substrate (1.524) and the relation between the critical angle and relative refractive index, the observed range of the critical angle corresponds to a cytoplasmic refractive index in the range 1.358–1.374. This range is similar to the values obtained for baby hamster kidney cells through reflection-interference microscopy (46). Immersion refractometry of mammalian cells in culture generally gives values near 1.36 for the average cytoplasmic index (3, 47, 48).

Ambrose (49) and Akatov et al. (50) have suggested that TIR refractometry be applied to the study of cell-substrate contact. In our experiments, the fluorescent dye in the mitochondrial compartment functions as a local detector of transmitted radiation. Under the conditions of measurement, the incidence angle 64.4° corresponds to an attenuation constant equal to 200 nm outside the contact zones; this is therefore an estimate of the minimum separation between mitochondria and substrate. The fluorescence of Hoescht dye 33342 in the nuclei of 3T3 cells also exhibited a sharp cut-on very close to the critical angle rather than a graded fluorescence expected for TIR illumination.

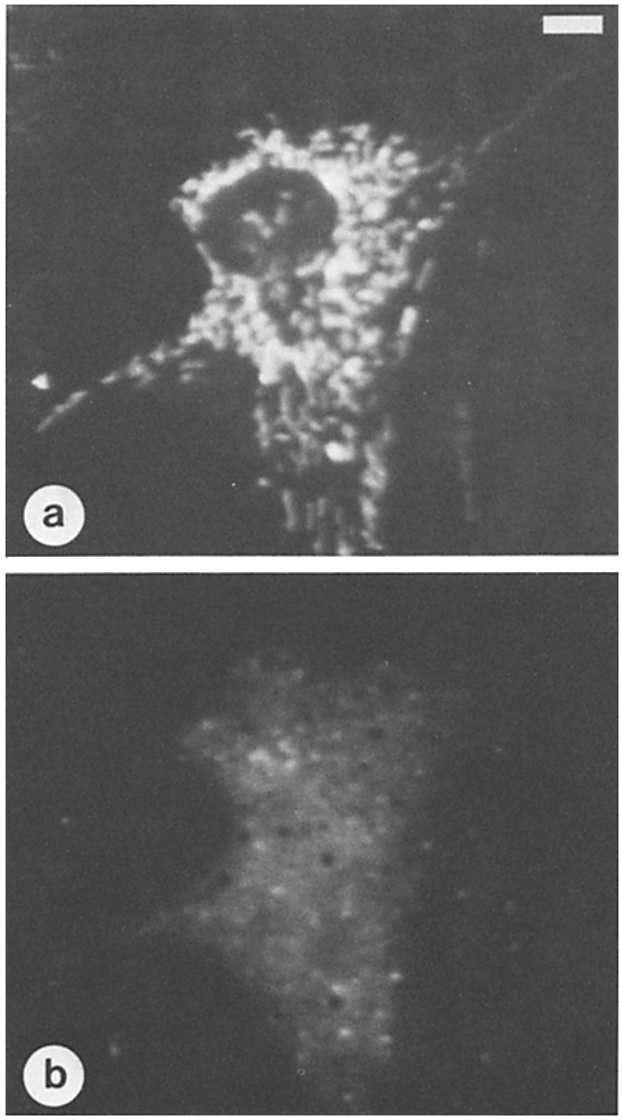

FIGURE 2 Fluorescence and TIRF images of 3T3 cell stained with dil-C_3-(3). Cells were stained at 37°C as described in Materials and Methods with the cationic indocarbocyanine dye dil-C_3-(3), which accumulates in electronegative compartments. (*a*) Fluorescence image of 3T3 cell showing mitochondria. (*b*) TIRF image. Field-attenuation constant 100 nm. Bar, 10 μm.

Correspondence of TIRF and Reflection-Interference Images

In all cases studied, the TIRF images of membrane, cytoplasmic compartment, microinjected AF-actin, and carboxyfluorescein in the external medium showed a high degree of pattern similarity to the corresponding zero-order reflection-interference image. Fig. 3 depicts the "red" TIRF image of the membrane of a 3T3 cell, the "green" image of cytoplasmic carboxyfluorescein, and the reflection-interference image, ob-

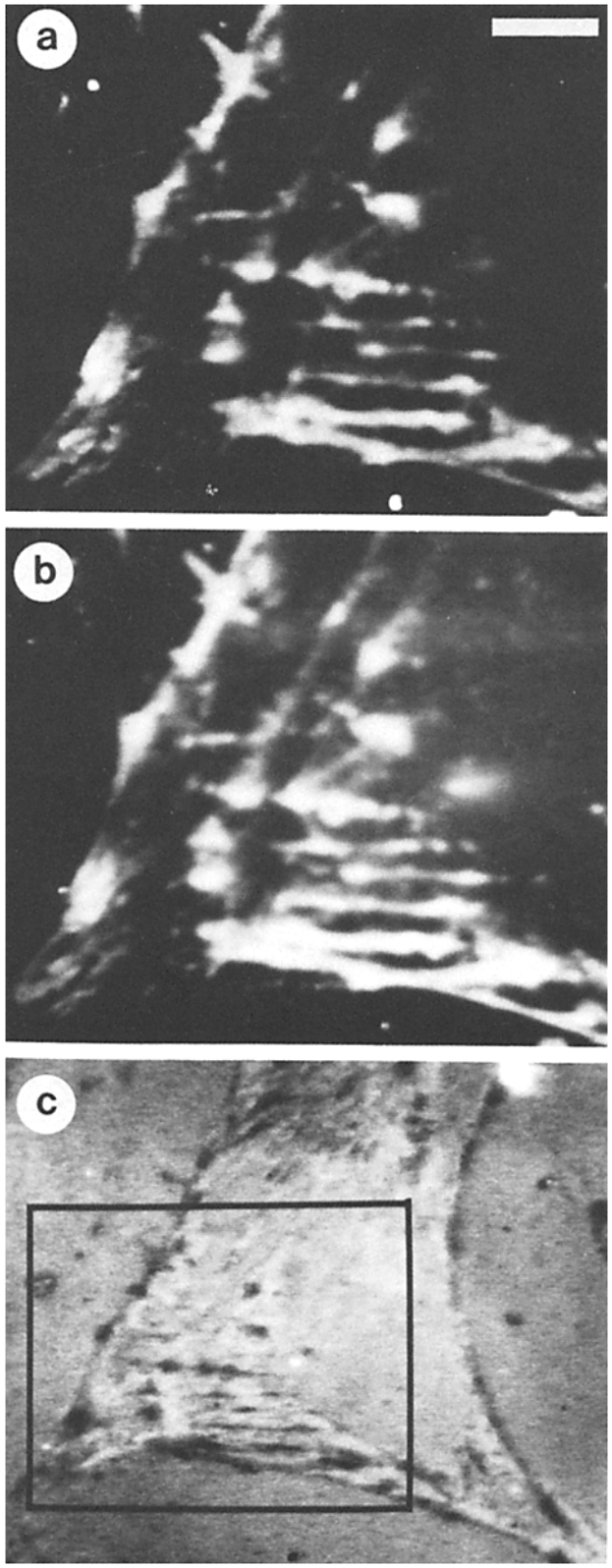

FIGURE 3 Correspondence of TIRF images of stained plasma membrane and cytoplasmic compartment of 3T3 cells. Cells were stained as described in Materials and Methods with the membrane-impermeable indocarbocyanine dye dil-C_{18}-(3), which labels the plasma membrane. (*a*) TIRF image, excited at 514 nm, emission band: >580 nm. The cells were then stained in situ with carboxyfluorescein diacetate. (*b*) TIRF image, excited at 488 nm, emission band: 520–560 nm. (*c*) Reflection-interference image of cell. TIRF images are 1.6 × enlargements relative to (*c*). Evanescent-field attenuation constants, 73 nm (at 488 nm excitation) and 75 nm (at 514-nm excitation). Bar, 10 μm.

tained as outlined in Materials and Methods. As expected on the basis of TIRF theory, the surface-TIRF and volume-TIRF images show the same pattern of contact with the substrate. The low-reflectance regions of the interference image were found to correspond one-to-one with the bright features of the TIRF images.

Distance Measurement by TIRF Photometry

The average value of F(2)/F(1), the emission ratio for low (2) and high (1) excitation angles-of-incidence was equal to 3.60 ± 0.40 (SD) for close-contact zones (eight cells), and was equal to 3.41 ± 0.38 (SD) for focal-contact zones (six cells). The computation of z_2 was performed for both of these ratios, using 1.5162, 1.335, 1.400, and 1.374 for the refractive indices of substrate, medium, membrane, and cytoplasm, respectively. The maximum observed value for the average index of 3T3 cytoplasm was used because this gave the smallest values for z_2, the distance between the substrate and plasma membrane; 69 nm for close-contact zones and 49 nm for focal-contact zones. At focal contacts, where the concentration of structural protein is known to be greater than average (4, 46), n_3 will be greater than 1.374. If n_3 is given the value 1.38, as measured by Bereiter-Hahn et al. (46) for the refractive index of focal contacts, the computed average distance between substrate and cytoplasm would be significantly less.

Contact Regions of Adherent and Motile Cells

The TIRF images of AF-actin, carboxyfluorescein, and FTC-dextran in interphase 3T3 cells fell into two categories that corresponded generally with morphological classification as motile or stationary. Cells classified as stationary (Figs. 4 and 5) were typically well spread with a cuspate periphery. The fluorescence image of AF-actin in this type of cell generally showed several prominent stress fibers. Motile cells (Figs. 6 and 7) had usually one convex segment of periphery that could be classified as a leading edge or lamellum and one or more regions of retraction. No fibers were observed by fluorescence of AF-actin in cells of this type.

Close- and focal-contact regions as defined by Izzard and Lochner (3) were found in both cell types by reflection-interference microscopy. Focal contacts were more numerous in cells of stationary morphology in which they often occurred in pairs that presumably were the opposite ends of stress fibers.

The AF-actin TIRF image of a typical stationary cell (Fig. 5*B*) showed compact, intensely fluorescent regions that corresponded one-to-one with focal contacts. Extended mottled patches of weaker fluorescence matched the close-contact structure of the cell. The fluorescence image of the same cell (Fig. 5*A*) showed that, as expected, a fluorescent stress fiber generally spanned two appropriately oriented zones of focal TIRF.

The TIRF images of stationary cells loaded with FTC-dextran or carboxyfluorescein had both focal and patchy features in common with actin images (Fig. 4*B*), even though stress fibers and other cytoskeletal structures did not become specifically labeled by these probes. Also in this case, a one-to-one relationship was found between locations of intense TIRF and focal contacts.

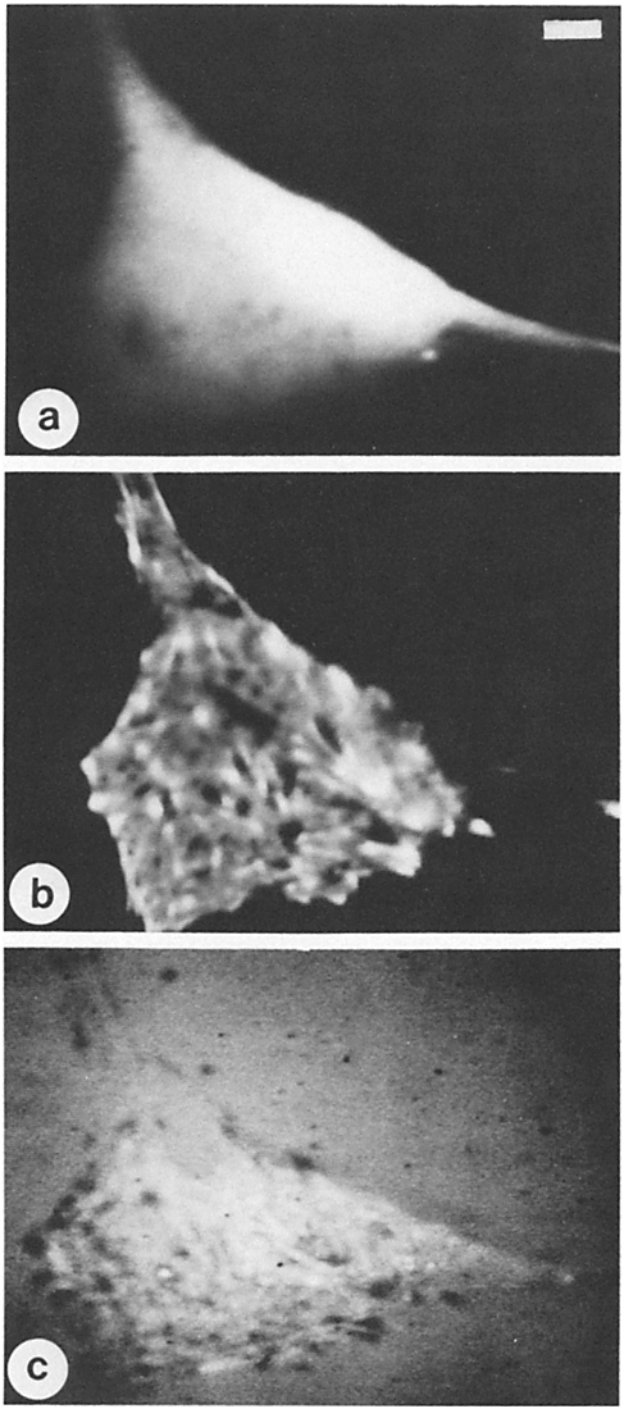

FIGURE 4 Stationary 3T3 cell containing carboxyfluorescein in the cytoplasmic compartment. Cells were stained with carboxyfluorescein diacetate as outlined in Materials and Methods. (*a*) Fluorescence image; (*b*) TIRF image; (*c*) reflection-interference image. Evanescent-field attenuation constant, 60 nm. Bar, 10 μm.

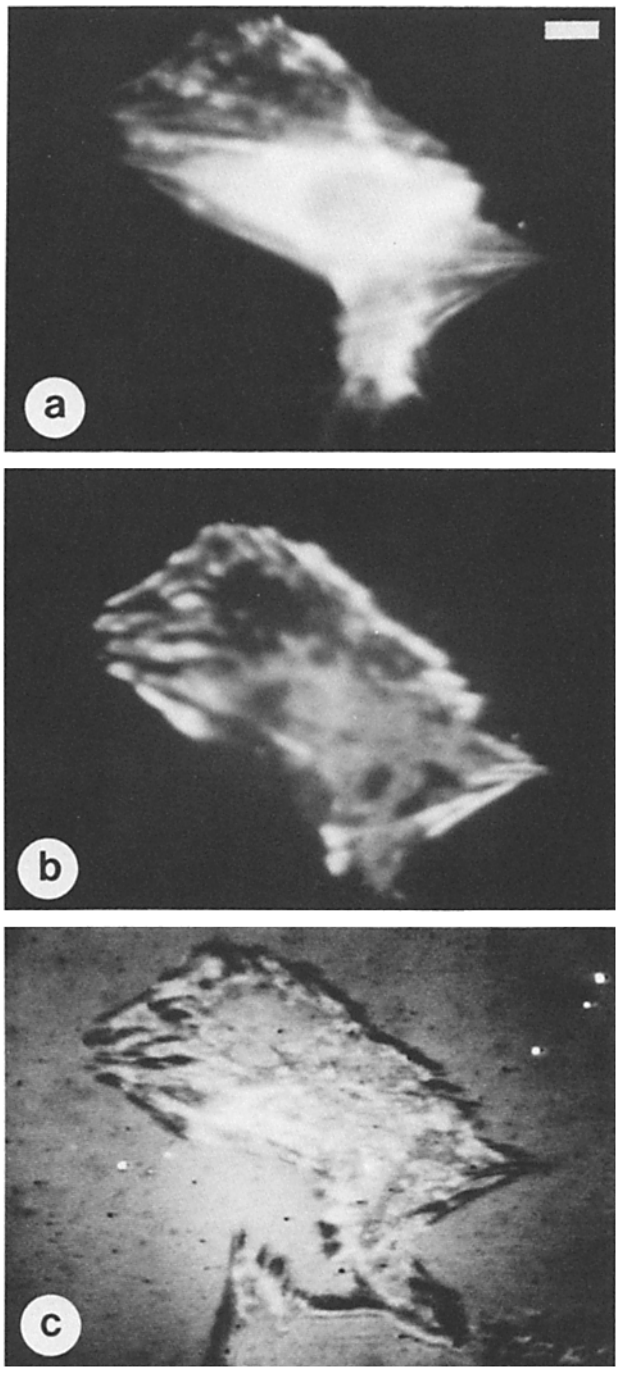

FIGURE 5 Stationary 3T3 cell containing AF-actin. Cell was microinjected as described in Materials and Methods. (*a*) Fluorescence image; (*b*) TIRF image; (*c*) reflection-interference image. Evanescent-field attenuation constant, 60 nm. Bar, 10 μm.

The pattern of fluorescence in the TIRF images of motile cells loaded with AF-actin or FTC-dextran closely matched the pattern of contacts in the respective reflection-interference images (Figs. 6 and 7). Generally, such cells displayed extensive areas of close contact. Leading lamellae, which had a low intensity in the fluorescence image due to extreme thinness, were of average or outstanding intensity in TIRF images (Figs. 6*B* and 7*B*). This result demonstrates that the concentration of the fluorescent species in the cytoplasm does not differ greatly between the contact regions of the lamellum and contact regions of the cell body. In the case of AF-actin, it was found that the intensely fluorescent ruffling zone sometimes present at the edge of the lamellum (Fig. 7*A*) was not distinguishable from other close-contact areas in the TIRF image (Fig. 7*B*). This result suggests that increased cytoplasmic thickness, not local concentration of actin, is responsible for this feature of the fluorescence image. Alternatively, it can be concluded that any concentration of actin significantly above average in the lamellum does not occur at the ventral surface.

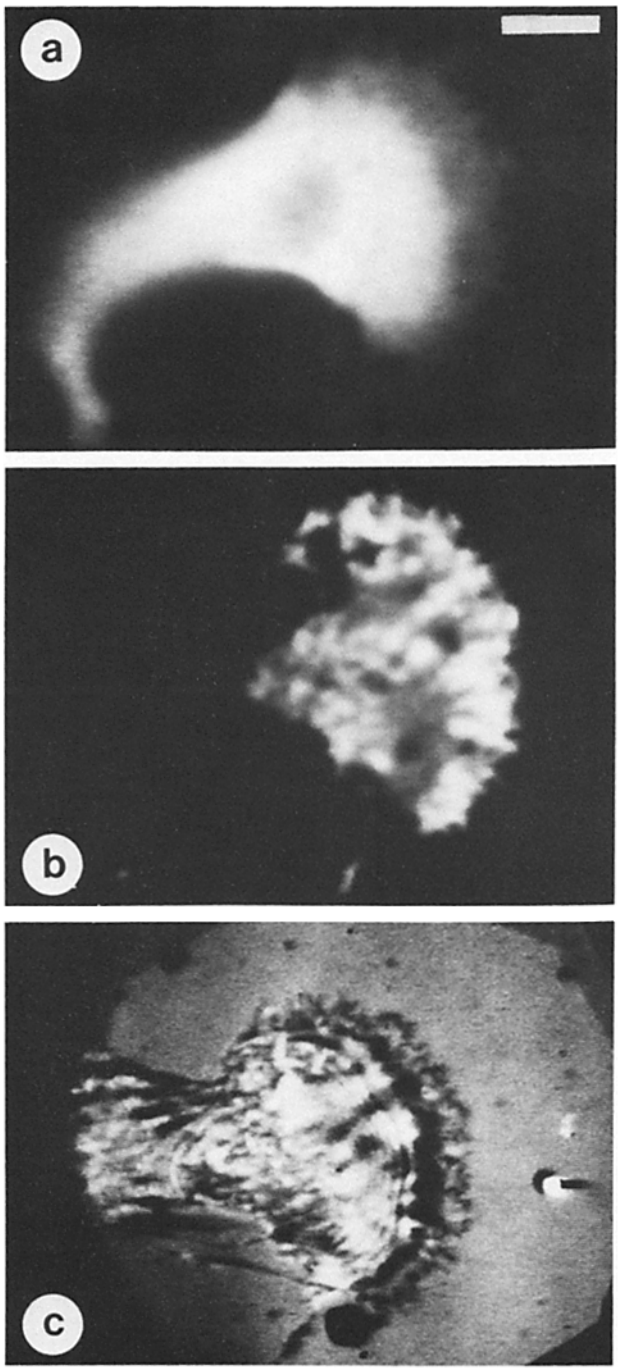

FIGURE 6 Motile 3T3 cell containing FTC-Dextran. Cell was scrape-loaded with fluorescent dextran and replated on the day before the experiment (see reference in Materials and Methods). (*a*) Fluorescence image; (*b*) TIRF image; (*c*) reflection-interference image. In *c*, the dark patches in the trailing part of the cell (left of center in photograph) were due to interference of light reflected from retraction fibers that were well above the substrate, and therefore do not represent locations of contact. This is confirmed by an absence of TIRF emission in *b*. Evanescent-field attenuation constant, 60 nm. Bar, 10 μm.

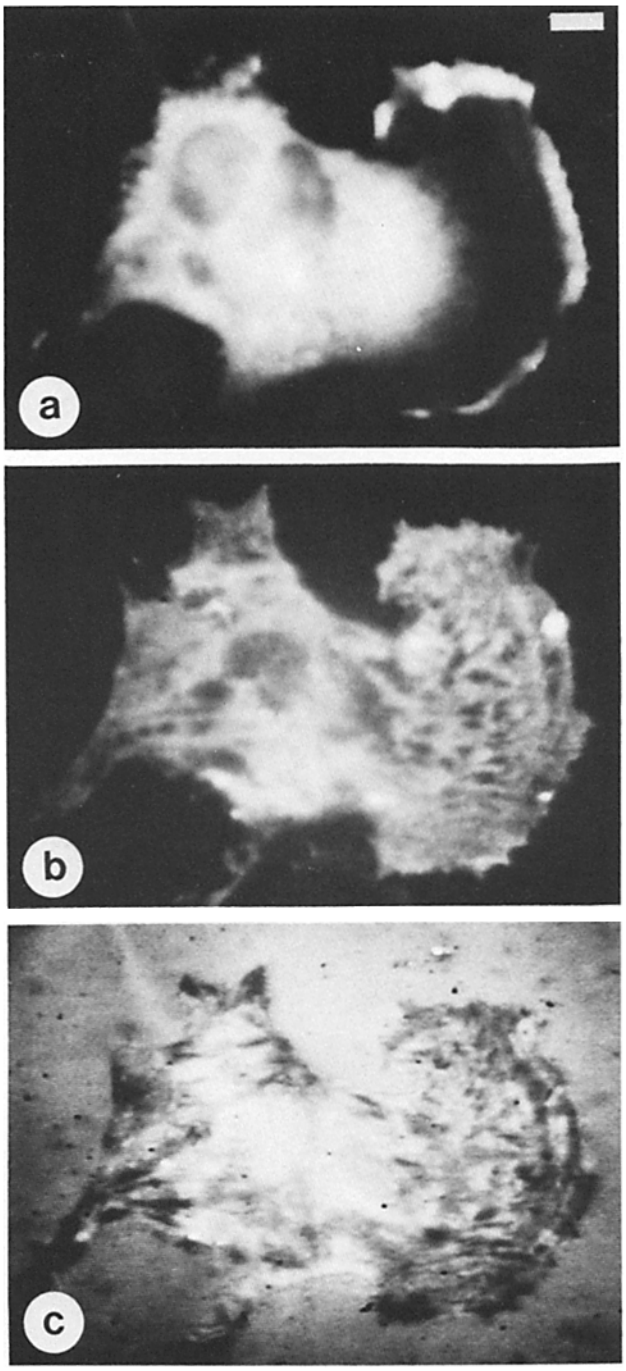

FIGURE 7 Motile 3T3 cell containing AF-actin. Cell was microinjected as described in Materials and Methods. (*a*) Fluorescence image; (*b*) TIRF image; (*c*) reflection-interference image. Evanescent-field attenuation constant, 60 nm. Bar, 10 μm.

Distribution of Actin in Motility

Time-lapse images of motile 3T3 cells showed that significant changes occurred in the distribution of AF-actin in peripheral contact regions over intervals of 15 min at 36°C (Fig. 8). Spreading and retraction of cytoplasmic processes at the cell perimeter was best visualized by TIRF. Transient lamellipodia, which were very thin and only faint components of the fluorescence image, were no less intense than other more static contact regions by TIR fluorescence (Fig. 8, B and E). Conversely, the fluorescence image of the cell showed various compact regions of intense fluorescence on the periphery which did not correspond one-to-one with regions of high TIRF emission. Newly formed processes that were visible by TIRF also were visible by reflection-interference as close-contact regions, with occasional small focal patches.

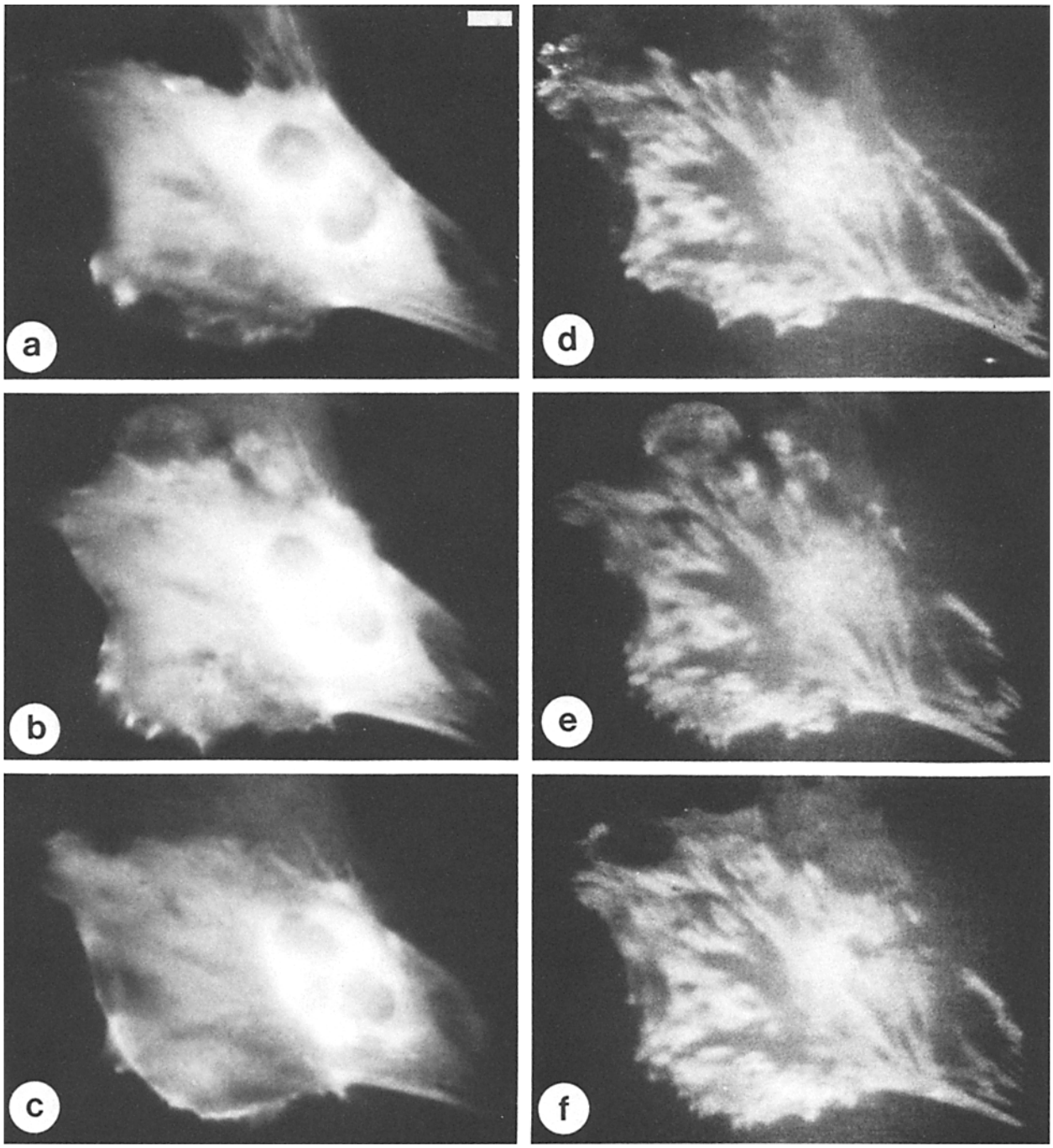

FIGURE 8 Time-lapse record of redistribution of AF-actin in a 3T3 cell at 36°C. Cell was microinjected as described in Materials and Methods. Discrete time-lapse recordings of fluorescence, TIRF, and reflection-interference images were made in rapid succession at 15-min intervals. *a* and *d* Fluorescence and TIRF images, respectively, at $t = 0$ (4 h postinjection). (*b* and e) As above, but at $t = 15$ min. (*c* and *f*) As above, but at $t = 30$ min. Evanescent-field attenuation constant, 60 nm. Bar, 10 μm.

The molecular specificity of fluorescence labeling in general, and the spatial specificity of TIRF in particular, suggest further simple measurements that could be made to quantify the concentration of actin in the contact region of a cell relative to its average concentration.

DISCUSSION

TIRF microscopy, as described by Axelrod (33), provides a way to locate regions of an adherent cell in which a specifically stained organelle or compartment is closely apposed to the substrate. Our data show that there is a very good correspondence between the close and focal contacts of the reflection-interference image and the TIRF image of 3T3 cells stained or loaded with diI-C_{18}-(3) (plasma membrane), carboxyfluorescein (cytoplasm), FTC-dextran (cytoplasm), or AF-actin. Even a water-soluble membrane-impermeable stain such as carboxyfluorescein, when added to the external solution, gives a reverse-contrast TIRF image of cell contacts that matches the interference image. The particular feature of TIRF microscopy that makes it very useful is the selectivity conferred by fluorescence labeling of a single molecular species; the

TIRF image then is a map of only that component in contact regions.

Location of Mitochondria and Nuclei Relative to the Substrate

The results obtained with the mitochondrial stain dil-C_3-(3) and the nuclear stain Hoechst 33342 demonstrate that neither class of organelle is a component of the cell contact regions. Our measurements set a limit of 200 nm as the closest possible apposition of mitochondria and substrate. We conclude that the laminar region of the cell between the substrate and the mitochondria excludes these organelles, and that this exclusion is most likely due to a laminar cytoskeletal matrix.

Because of their distance from the substrate, stained mitochondria are sensitive indicators of the glass/cytoplasm critical angle. Our results for the average cytoplasmic refractive index of 3T3 cells fall in the range found for other cell types. Currently, the greatest source of error in our TIR measurements is in the determination of the true angle of incidence, since factors such as prism leveling and the prism/specimen corner angle are not controlled precisely. The estimated systematic angular error for our current TIRF microscope is ±0.25°.

Factors Affecting TIRF Intensity

In the interpretation of TIRF images, three factors must be taken into consideration: proximity to substrate, dye concentration, and refractive index. Variations in refractive index within the specimen will be of two types. An index variation normal to the substrate results from the laminar structure of the specimen which in the simplest case consists of the layers glass:medium:membrane:cytoplasm. This complicates the form of the evanescent field and its dependence on incidence angle in a predictable way. At this point in our research we have used a four-layer model in which the membrane is treated as a 4-nm layer of hydrocarbon. Lateral variation of refractive index occurs because cytoplasm is not a homogeneous substance. Contact regions which are the termination points of fibers have a significantly higher protein concentration than average. Bereiter-Hahn et al. (46) have found the typical index at focal contacts to be 1.38–1.40 and that of bulk cytoplasm to be approximately 1.36 for several cell types. Refractive index affects both the penetration and strength of the evanescent field in the specimen, and therefore the TIRF emission rate. There is a strong effect on TIRF emission rate. The use of 1.40 as the cytoplasmic index reduces the computed value of z_2 by ~70% relative to the values we report. Likewise, dispensing with the multilayer optical model and treating the specimen as a homogenous dielectric of index 1.36 results in a 30–60% increase in the computed distances. Although it would be attractive to report here values of z_2 computed using a high cytoplasmic index, our own measurements (by TIRF refractometry) give us a more limited range and we have chosen to use an index in that range (1.374) for the analysis reported here.

Refractive index inhomogeneities also give rise to light scattered from the evanescent field. Close to the critical angle this radiation will account for significant excitation of fluorescence in the specimen. The internal control for the effect of light scattering in these experiments was the observation that TIRF emission from noncontact regions of the cell was always much less than from the contact regions. This means that the average intensity in the bulk of the specimen due to scatter originating near the interface is very low. The observation does not imply that the short-range fields of the scatterers are weak at distances comparable to $d(\theta)$. This stronger conclusion was reached on the basis of a calculation discussed in *Theory and TIRF Instrumentation.*

In cell-substrate contact regions, variations in fluorescent probe concentration will arise through exclusion and chemical affinity. At locations of very high protein concentration, such as in a cytoplasmic fiber, the solvent volume will be significantly lower than average. A fiber refractive index of 1.39 is equivalent to a protein concentration of 33%, or a solvent volume fraction of 0.76, compared with 0.88 for the average. A small dye molecule such as carboxyfluorescein would then have a total concentration in the dense phase equal to 0.76/0.88 = 0.86 of the dilute phase concentration. This exclusion effect would be compensated to some extent by the greater refractive index of dense-contact structures. A large molecule such as FTC-dextran would be distributed more unevenly than free dye under conditions in which the size of the solvent regions in the dense phase was comparable to or smaller than the radius-of-gyration (R_G) of the polymer. For the dextran used here (average molecular weight = 6.6×10^4), R_G is ~90 Å (51), which is on the order of the spacing of filaments in cytoplasmic fibers (52). Experiments are in progress to define the steric parameters of cytoskeletal elements in living cells by measurement of exclusion.

In the case of actin, assembly into cytoskeletal structures leads to concentration of the protein, potentially to a much higher level than in bulk cytoplasm. An estimate of 10 mg/ml as the cytoplasmic actin concentration, and the assumption that a fiber of 33% protein content is 50% actin, give the result that actin is 16-fold more concentrated in the fiber. Because AF-actin appears to react in much the same way as native actin, the fluorescence of the fiber should reflect the high concentration of actin in it.

Distance between Substrate and Membrane

Reflection-interference microscopy has been used previously to estimate the distance between cell and substrate in contact zones. In the analysis of reflection-interference data, as in the analysis of TIRF data, the derived distances are affected by the values of the refractive index parameters used in computation. The three-layer model used by Izzard and Lochner (3), in which the cell is assigned a single index and variations in reflectivity assigned entirely to variation in the cell-to-substrate distance, gives the result that the film of culture medium between cell and substrate is <50 nm thick at close contacts, and ~10 nm thick at focal contacts. At the other extreme, Bereiter-Hahn et al. (46) used a two-layer optical model of close apposition in which reflectivity was a function of local cytoplasmic refractive index.

Our results, that the average value of z_2 is 69 nm in close-contact zones and is 49 nm at focal contacts, also derive from use of a particular set of refractive indices in a multilayer model. Some of these indices, such as for the substrate and for cytoplasm, were measured directly. The index of the plasma membrane was estimated from that of long-chain hydrocarbon. Likewise, the index of the fluid phase between cell and slide was estimated from the measured index of culture medium. The cytoplasmic index at contact sites was set equal to the maximum measured average, even though there are several lines of evidence, both optical and electron

microscopic, that indicate a greater density of protein in these zones. Comparison of TIRF and reflection-interference distances will be possible when both measurements are made on the same cell. A further improvement in technique would result from measuring the cytoplasmic refractive index of each cell by TIRF refractometry rather than using an average index for all cells and for all contact zones of each cell.

The exponential form of the relation between z_2 and the measured fluorescence $F(\theta)$ (see Appendix) gives an essentially constant additive error in z_2 for any inaccuracy in the index or angle parameters. The difference of 20 nm between z_2 at close contacts and at focal contacts should therefore be a good estimate of the difference in membrane-substrate separation at these two types of attachments. An additive error will also not greatly affect the ordering of different contact-zone proteins, such as actin and vinculin, since the parameter of interest in such experiments would be the difference between the distances measured from substrate to each protein fluorescent analog in the cytoplasm.

Interpretation of TIRF Images

The results of two-angle TIRF photometry of selected contact regions of 3T3 cells show that the boundary of the cytoplasmic compartment of these cells is within a distance of the substrate given by the value of the evanescent-field attenuation constant. From the preceding discussion and estimates of the effects of refractive index and concentration, we can draw several conclusions about TIRF images.

In the range of focal and close contacts, the effects of variable refractive index alone may cause a 50% variation in TIRF intensity. This does not account for the much larger range of intensity actually observed. The effect of exclusion is also small in the case of carboxyfluorescein trapped in the cytoplasm, but possibly much larger in the case of FTC-dextran. Since TIRF images of these two probes in 3T3 cells are generally indistinguishable, we conclude that exclusion is also not a large effect for the 70,000-mol-wt polymer. Therefore, our first major conclusion is that single TIRF images of these volume marker molecules are principally maps of only the proximity of substrate and cytoplasmic compartment.

In the case of AF-actin in vivo, both proximity and local concentration are significant parameters in the TIRF image. Ideally, multi-angle TIRF photometric measurements of selected contact zones provide the information from which the separation of AF-actin and substrate can be computed. In practice, we found that photobleaching of AF-actin in focal-contact regions necessitated the use of lower excitation intensity than the sensitivity of our photometer currently permits. Presumably, photobleaching also occurs during TIRF photometry of intracellular FTC-dextran and carboxyfluorescein. In this case, there is apparently rapid exchange of unbleached material into the contact regions from the large reservoir represented by the volume of the cell above the contact region, so that the emission rate is constant. This observation suggests that fluorescence photobleaching recovery measurements performed in the TIR mode (53) would be a way of characterizing the assembly state of actin in cell-contact zones.

Contact-region Actin and Motility

One of the results of examining a large number of cells injected with AF-actin is that cells having unmistakably motile morphology also showed even, or evenly mottled, TIRF emission over large close-contact areas. In some cases this pattern extended over the entire projection of the cell (Fig. 7*B*). This suggests that the operation of the cytoplasmic motile apparatus does not depend upon an asymmetric or polarized distribution of contact region actin. An important step would be measurement of the photobleaching recovery rate of close-contact actin in the lamellum and tail of such a cell, since the images presented here do not indicate the assembly state of the actin.

Time-lapse TIRF images of AF-actin show the rapid extension (and retraction) of lamellae. These motile structures appear to form directly as a spreading close-contact zone. The concentration of actin in these structures does not appear to be significantly different from that in more static close-contact regions farther from the periphery of the cell.

The selectivity conferred by the use of fluorescence in TIR microscopy allows the spatial organization of cell-contact regions to be studied. In general, several types of TIR and TIRF measurements must be made in order to analyze the contribution of proximity, concentration, and refractive index to the TIRF image of a live cell. At the most simple level, we have demonstrated that the TIRF image of FTC-dextran or carboxyfluorescein in the cytoplasm of a cell is principally a map of cell-substrate proximity. Refractive index, and its lateral variation, can be measured by TIRF photometry as described here, or by photometry of light scattered from the evanescent field as outlined by Akatov et al. (50). In a given cell-contact region, proximity can be computed from TIRF measurements at two incidence angles of a single fluorescent species. Therefore it should be possible to compare proximity to the substrate for actin and other protein species of the contact region such as vinculin in vivo.

In addition to elucidating the molecular composition and ordering of cell contact regions in vivo, TIRF photobleaching recovery could be measured to compare the translational mobility of protein components of the contact region to the mobility of a test molecule such as dextran that has no particular affinity for the cytoskeleton.

APPENDIX

Multilayer Optical Model for TIRF Microphotometry

In the instrument constructed for these experiments, s-polarized, collimated, coherent light propagating in a glass prism optically coupled to a microscope slide, is incident at high angle upon the planar interface between slide and specimen (Fig. 1). We assume that the specimen is stratified; i.e., consists of layers parallel to the interface, each of which may have a different refractive index (with the slide index being n_1), different thickness, and different fluorescent-probe content. The model used here for data analysis consists of four dielectric layers: the glass slide ($n_1 = 1.5162$), the film of liquid culture medium ($n_2 = 1.335$) of thickness z_2, the bilayer plasma membrane ($n_3 = 1.400$) of thickness z_3 (here set equal to 4.0 nm), and the cytoplasm ($n_4 = 1.374$).

The solution of Maxwell's equations for plane waves in this multilayer system gives the amplitude, phase, and propagation vector for the fields in each layer. The complex amplitudes can be derived by straightforward but tedious algebra; the result of interest is e°_4, the complex amplitude at the membrane-cytoplasm interface beyond which the fluorescent dye molecules are located in our specimen. For incident unit-amplitude s-polarized plane waves in layer 1:

$$e^{\circ}_4 = \frac{T_{12}T_{23}T_{34}e^{i(k_{z2}-k_{z4})z_2}\, e^{i(k_{z3}-k_{z4})z_3}}{1 + R_{12}R_{23}(e^{i2k_{z2}z_2}) + R_{23}R_{34}(e^{i2k_{z3}z_3}) + R_{34}R_{12}(e^{i2k_{z2}z_2})(e^{i2k_{z3}z_3})},$$

In the above equation, T_{ij} is the Fresnel transmission coefficient for s-polarized waves at the interface between layers i and j. R_{ij} is the corresponding reflection coefficient. z_2 and z_3 are the thicknesses of layers 2 and 3, respectively; $z_2 + z_3$, therefore, is the total distance between the substrate and the cytoplasmic

compartment. k_{z2}, k_{z3}, and k_{z4} are the z-components (normal to the layers) of the propagation vector in each layer: $k_{zj} = i(k''_{zj}) = i(2\pi/\lambda_0)(n_1^2\sin^2\theta_1 - n_j^2)^{1/2}$, for $\theta_1 \geq \theta_{cj}$ (the critical angle for layers 1 and j).

The full expression for the field in layer 4 is $e_4 = e^\circ_4 e^{i(k_{x4}x + k_{z4}z)}$, where k_{x4} is always a real number and k_{z4} is imaginary. The intensity in layer 4 is proportional to the square norm of e_4: $|e_4|^2 = |e^\circ_4|^2\, e^{-2(k''_{z4})z}$ or $I_4(z) = I^\circ_4 e^{-z/d_{14}}$, for $z \geq z_2 + z_3$, where $I^\circ_4 = |e^\circ_4|^2$, and where $d_{14} = 1/2(k''_{z4}) = \lambda_0/4\pi(n_1^2\sin^2\theta_1 - n_4^2)^{1/2}$. Analogous equations for a single dielectric interface are given in the text as Eqs. 1 and 2. In the expression for e°_4, only the first and third terms of the denominator are significant for the indices used.

In our cellular specimens, the fluorescent dye molecules are in the cytoplasmic compartment, which corresponds to dielectric 4 in the optical model. The fluorescence emission will therefore be proportional to the integrated product of dye concentration (c_0), excitation intensity, $I_4(z)$, and a weighting function $W(z)$ that gives the fraction of emitted power that is not carried by evanescent waves coupled to plane waves in the microscope slide: these waves, which propagate away from the microscope aperture on the specimen side of the interface, do not contribute to the measured intensity. The fraction of the remaining radiated power that enters the microscope aperture is a weak function of emitter distance to the interface (z). This is because of the relatively low reflectivity of the slide/specimen interface (see main text for further discussion). $W(z)$ is a function only of the relative refractive index of specimen and substrate, and of the emission wavelength. We have approximated $W(z)$ by using 1.52 as the substrate index, 1.33 for the mean specimen index, and 500 nm as the emission wavelength. The mathematical form of $W(z)$ can be derived from expressions given by Lukosz and Kunz (40, 43): $W(z) = 1 + \sum_{i=1}^{4} a_i e^{-b_i z}$, where the a_i are functions only of refractive index, and the b_i are functions of refractive index multiplied by $4\pi/\lambda$. $W(z)$ is also a function of the type of emitting dipole (electric or magnetic), and its orientation relative to the interface. The coefficients used in our computations are those for randomly oriented electric dipoles, the situation that most likely represents carboxyfluorescein or fluorescein-dextran in our specimens. Therefore,

$$F(\theta) = K \int_{z_2+z_3}^{\infty} c_0 I_4(\theta, z) W(z) dz;$$

$$F(\theta) = K c_0 |e^\circ_4(\theta)|^2 \int_{z_2+z_3}^{\infty} e^{-z/d_{14}(\theta)} \left(1 + \sum_{1}^{4} a_i e^{-b_i z}\right) dz;$$

$$F(\theta) = K c_0 |e^\circ_4(\theta)|^2 d_{14}(\theta) \left(1 + \sum_{1}^{4} \frac{a_i e^{-b_i(z_2+z_3)}}{1 + b_i d_{14}(\theta)}\right) e^{-(z_2+z_3)/d_{14}(\theta)}.$$

From this result, it can be seen that the ratio of two measurements $F(\theta_1)$ and $F(\theta_2)$ (abbreviated $F(2)/F(1)$ in the text) will be independent of the factor Kc_0, and a function of z_2 and z_3 through the factors e°_4 and the exponential terms. In practice, the above expression was evaluated for a series of values for $z_2 + z_3$ with $z_3 = 4.0$ nm, and the results graphed. As described in Materials and Methods, our data was averaged as the ratio $F(2)/F(1)$; the corresponding value of $z_2 + z_3$ was read from the graph. The reported values of z_2 are equal to $(z_2 + z_3) - 4.0$ nm. The correction for coupling of evanescent emission to the substrate accounts for a correction of ~6 nm in this case. More accurate expressions for $W(z)$ that account for the multilayer structure of the specimen and the perturbation of the emission field due to reflection at the interfaces could be derived, but the resulting increase in complexity is not warranted at this point, given the uncertainty in some of the refractive index parameters of the optical model.

We thank Dr. Katherine Luby-Phelps for aid in translation of Akatov et al. (50) into English, Keiko Ozaki for the preparation of fluorescent actin, and Dr. Philip Amato for microinjection of actin into cells used in these experiments.

This research was supported by a grant from the Council for Tobacco Research-USA (#1412).

Received for publication 16 May 1984, and in revised form 26 November 1984.

REFERENCES

1. Curtis, A. S. G. 1964. The mechanism of adhesion of cells to glass: a study by interference reflection microscopy. *J. Cell Biol.* 20:199–215.
2. Lochner, L., and C. S. Izzard. 1973. Dynamic aspects of cell-substrate contact in fibroblast motility. *J. Cell Biol.* 59 (2, Pt. 2):199*a*. (Abstr.)
3. Izzard, C. S., and L. R. Lochner. 1976. Cell-to-substrate contacts in living fibroblasts: an interference reflexion study with an evaluation of the technique. *J. Cell Sci.* 21:129–159.
4. Abercrombie, M., J. E. M. Heaysman, and S. M. Pegrum. 1971. The locomotion of fibroblasts in culture. IV. Electron microscopy of the leading lamella. *Exp. Cell Res.* 67:359–367.
5. Geiger, B. 1983. Membrane-cytoskeleton interaction. *Biochem. Biophys. Acta.* 737:305–341.
6. Heath, J. P., and G. A. Dunn. 1978. Cell to substratum contacts of chick fibroblasts and their relation to the microfilament system. A correlated interference-reflexion and high-voltage electron-microscope study. *J. Cell Sci.* 29:197–212.
7. Geiger, B. 1979. A 130K Protein from chicken gizzard: its localization at the termini of microfilament bundles in cultured chicken cells. *Cell.* 18:193–205.
8. Wehland, J., M. Osborn, and K. Weber. 1979. Cell-to-substratum contacts in living cells: a direct correlation between interference-reflexion and indirect-immunofluorescence microscopy using antibodies against actin and α-actinin. *J. Cell Sci.* 37:257–273.
9. Kreis, T. E., K. M. Winterhalter, and W. Birchmeier. 1979. In vivo distribution and turnover of fluorescently labeled actin microinjected into human fibroblasts. *Proc. Natl. Acad. Sci. USA.* 76:3814–3818.
10. Kreis, T. E., B. Geiger, and J. Schlessinger. 1982. Mobility of microinjected rhodamine actin within living chicken gizzard cells determined by fluorescence photobleaching recovery. *Cell.* 29:835–845.
11. Burridge, K., and J. R. Feramisco. 1980. Microinjection and localization of a 130K protein in living fibroblasts: a relationship to actin and fibronectin. *Cell.* 19:587–595.
12. Geiger, B., A. H. Dutton, K. T. Tokuyasu, and S. J. Singer. 1981. Immunoelectron microscope studies of membrane-microfilament interactions: distributions of α-actinin, tropomyosin, and vinculin in intestinal epithelial brush border and chicken gizzard smooth muscle cells. *J. Cell Biol.* 91:614–628.
13. Arndt-Jovin, D. J., and T. M. Jovin. 1977. Analysis and sorting of living cells according to deoxyribonucleic acid content. *J. Histochem. Cytochem.* 25:585–589.
14. Johnson, L. V., M. L. Walsh, and L. B. Chen. 1980. Localization of mitochondria in living cells with rhodamine 123. *Proc. Natl. Acad. Sci. USA.* 77:990–994.
15. Cohen, R. L., K. A. Muirhead, J. E. Gill, A. S. Waggoner, and P. K. Horan. 1981. A cyanine dye distinguishes between cycling and non-cycling fibroblasts. *Nature (Lond.).* 290:593–595.
16. Thomas, J. A., R. N. Buchsbaum, A. Zimniak, and E. Racker. 1979. Intracellular pH measurements in Ehrlich ascites tumor cells utilizing spectroscopic probes generated *in situ*. *Biochemistry.* 18:2210–2218.
17. Sims, P. J., A. S. Waggoner, C.-H. Wang, and J. F. Hoffman. 1974. Studies on the mechanism by which cyanine dyes measure membrane potential in red blood cells and phosphatidylcholine vesicles. *Biochemistry.* 13:3315–3330.
18. Waggoner, A. S., and A. Grinvald. 1977. Mechanisms of rapid optical changes of potential-sensitive dyes. *Ann. N. Y. Acad. Sci.* 303:217–241.
19. Kinnally, K. W., H. Tedeschi, and B. L. Maloff. 1978. Use of dyes to estimate the electrical potential of the mitochondrial membrane. *Biochemistry* 17:3419–3428.
20. Ohkuma, S., and B. Poole. 1978. Fluorescence probe measurement of the intralysosomal pH in living cells and the perturbation of pH by various agents. *Proc. Natl. Acad. Sci. USA.* 75:3327–3331.
21. Tsien, R. Y., T. Pozzan, and T. J. Rink. 1982. Calcium homeostasis in intact lymphocytes: cytoplasmic free calcium monitored with a new, intracellularly trapped fluorescent indicator. *J. Cell Biol.* 94:325–334.
22. Dolbeare, F. A. 1981. Fluorometric quantification of specific chemical species in single cells. In Modern Fluorescence Spectroscopy. E. L. Wehry, editor. Plenum Press, NY, New York. 251–293.
23. Taylor, D. L., and Y.-L. Wang. 1978. Molecular cytochemistry: incorporation of fluorescently labeled actin into living cells. *Proc. Natl. Acad. Sci. USA.* 75:857–861.
24. Wang, Y.-L., J. Heiple, and D. L. Taylor. 1982. Fluorescent analog cytochemistry of contractile proteins. *Methods Cell Biol.* 24B:1–11.
25. Taylor, D. L., P. A. Amato, K. Luby-Phelps, and P. McNeil. 1984. Fluorescent analog cytochemistry. *Trends Biochem. Sci.* 9(3):88–91.
26. Jacobson, K., E. Elson, D. Koppel, and W. Webb. 1983. International workshop on the application of fluorescence photobleaching techniques to problems in cell biology. *Fed. Proc.* 42:72–79.
27. Axelrod, D., N. L. Thompson, and T. P. Burghardt. 1983. Total internal reflection fluorescent microscopy. *J. Microsc.* 129:19–28.
28. Yguerabide, J., and M. C. Foster. 1981. Fluorescence spectroscopy of biological membranes. *In* Membrane Spectroscopy. E. Grell, editor. Springer-Verlag, 199–269.
29. Fernandez, S. M., and R. D. Berlin. 1976. Cell surface distribution of lectin receptors determined by resonance energy transfer. *Nature (Lond.).* 264:411–415.
30. Herman, B., and S. M. Fernandez. 1982. Dynamics and topographical distribution of surface glycoproteins during myoblast fusion: a resonance energy transfer study. *Biochemistry.* 21:3275–3283.
31. McNeil, P. L., L. Tanasugarn, J. B. Meigs, and D. L. Taylor. 1983. Acidification of phagosomes is initiated before lysosomal enzyme activity is detected. *J. Cell Biol.* 97:692–702.
32. Tanasugarn, L., P. L. McNeil, G. T. Reynolds, and D. L. Taylor. 1984. Microspectrofluorometry by digital image processing: measurement of cytoplasmic pH. *J. Cell Biol.* 98:717–724.
33. Axelrod, D. 1981. Cell-substrate contacts illuminated by total internal reflection fluorescence. *J. Cell Biol.* 89:141–145.
34. Wang, Y.-L., and D. L. Taylor. 1980. Preparation and characterization of a new molecular cytochemical probe: 5-iodoacetamidofluorescein-labeled actin. *J. Histochem. Cytochem.* 28:1198–1206.
35. Amato, P. A., E. R. Unanue, and D. L. Taylor. 1983. Distribution of actin in spreading macrophages: a comparative study on living and fixed cells. *J. Cell Biol.* 96:750–761.
36. McNeil, P. L., R. F. Murphy, F. Lanni, and D. L. Taylor. 1984. A method for incorporating macromolecules into adherent cells. *J. Cell Biol.* 98:1556–1564.
37. Stratton, J. A. 1941. Electromagnetic Theory. McGraw-Hill Book Co., Inc., New York, 497–500.
38. Harrick, N. J. 1967. Internal Reflection Spectroscopy. John Wiley and Sons, Wiley-Interscience, New York, 13–40.
39. Hirschfeld, T. 1965. Total reflection fluorescence (TRF). *Canadian Spectroscopy.* 10:128.
40. Lukosz, W., and R. E. Kunz. 1977. Light emission by magnetic and electric dipoles close to a plane interface. I. Total radiated power. *J. Opt. Soc. Am.* 67:1607–1614.
41. Lukosz, W., and R. E. Kunz. 1977. Light emission by magnetic and electric dipoles close to a plane dielectric interface. II. Radiation patterns of perpendicular oriented dipoles. *J. Opt. Soc. Am.* 67:1615–1619.
42. Carniglia, C. K., L. Mandel, and K. H. Drexhage. 1972. Absorption and emission of evanescent photons. *J. Opt. Soc. Am.* 62:479–486.
43. Lukosz, W., and R. E. Kunz. 1977. Fluorescence lifetime of magnetic and electric dipoles near a dielectric interface. *Optics Communications.* 20:195–199.

44. Gingell, D., and I. Todd. 1979. Interference reflection microscopy: a quantitative theory for image interpretation and its application to cell-substratum separation measurement. *Biophys. J.* 26:507–526.
45. Gingell, D. 1981. The interpretation of interference-reflection images of spread cells: significant contributions from thin peripheral cytoplasm. *J. Cell Sci.* 49:237–247.
46. Bereiter-Hahn, J., C. H. Fox, and B. Thorell. 1979. Quantitative reflection contrast microscopy of living cells. *J. Cell Biol.* 82:767–779.
47. Barer, R., K. F. A. Ross, and S. Tkaczyk. 1953. Refractometry of living cells. *Nature (Lond.).* 171:720–724.
48. Ross, K. F. A., and R. E. Gordon. 1982. Water in malignant tissue, measured by cell refractometry and nuclear magnetic resonance. *J. Microsc.* 128:7–21.
49. Ambrose, E. J. 1961. The movements of fibrocytes. *Exp. Cell Res.* 8 (*Suppl.*):54–73.
50. Akatov, V. S., A. A. Kudryavtsev, and E. I. Lezhnev. 1980. The use of the frustrated total reflection effect for studying the adhesion to glass of mammalian cells. I. Results of theoretical analysis. *Tsitologia.* 22:230–233.
51. Benoit, H. 1948. Calcul de l'ecart quadratique moyen entre les extremites de diverses chaines moleculaires de type usuel. *J. Polymer Sci.* 3:376–388.
52. Goldman, R. D., and D. M. Knipe. 1973. Functions of cytoplasmic fibers in non-muscle cell motility. *Cold Spring Harbor Symp. Quant. Biol.* 37:523–534.
53. Thompson, N. L., T. P. Burghardt, and D. Axelrod. 1981. Measuring surface dynamics of biomolecules by total internal reflection fluorescence with photobleaching recovery or correlation spectroscopy. *Biophys. J.* 33:435–453.